

Observation of modulational instability and Townes soliton formation in two-dimensional Bose gases

Cheng-An Chen¹ and Chen-Lung Hung^{1,2,*}

¹ Department of Physics and Astronomy, Purdue University, West Lafayette, IN 47907, USA and

² Purdue Quantum Science and Engineering Institute,
Purdue University, West Lafayette, IN 47907, USA

(Dated: June 16, 2022)

We experimentally study the non-equilibrium dynamics of two-dimensional atomic Bose gases quenched from repulsive to attractive interactions. We observe the manifestation of modulational instability that, instead of causing collapse, fragments a large two-dimensional superfluid into multiple wave packets universally around a threshold atom number necessary for the formation of Townes solitons. We confirm that the density distributions of quench-induced solitary waves are in excellent agreement with the stationary Townes profiles. Furthermore, our density measurements in space and time domain reveal detailed information about this dynamical process, from the hyperbolic growth of density waves, the formation of solitons, to the subsequent collision and collapse dynamics, demonstrating multiple universal behaviors in an attractive many-body system in association with the formation of a quasi-stationary state.

I. INTRODUCTION

Predicting the evolution of nonlinear systems under attractive interactions is a challenging task, owing to the instability to collapse [1–3]. Bright solitons are remarkable stationary states, established when the self-focusing effect responsible for collapse is exactly compensated by wave dispersion [4, 5]. In uniform two-dimensional (2D) systems with standard cubic interactions, such as Kerr medium [3, 6] or matter-waves formed by weakly interacting 2D Bose gases [7, 8], however, such intricate balance cannot be fulfilled except when a wave packet possesses a critical norm (or total atom number) known as the Townes threshold and a specific waveform known as the Townes profile [6, 9, 10] – only at which bright solitons can form. A Townes soliton is predicted to be unstable as long as the norm deviates from the Townes threshold [3, 9], or when its density distribution is perturbed away from the Townes profile. Despite extensive interests in multidimensional bright solitons [9–13], including recent advancements on 2D spatial solitons in various nonlinear optics settings [3, 11, 14], an experimental realization and characterization of Townes solitons has remained elusive.

In soliton formation dynamics, modulational instability (MI) is a ubiquitous mechanism that causes the amplification of initial wave disturbances and fragmentation into solitary waves [1, 15–19]. In one-dimensional (1D) systems, MI is responsible for the formation of stable soliton trains, for example, in nonlinear fiber optics [20–22], in 1D Bose gases [18, 19, 23, 24], or in Bose-Einstein condensates in optical lattices [25–27]. In higher spatial-dimensions, transverse MI and wave fragmentation were studied in various types of bulk nonlinear optical media [14, 28–30]. However, detailed dynamics of multidimensional MI and its possible connection to the formation

of a quasi-stationary state, the unstable Townes solitons, have not been clearly demonstrated.

Using ultracold 2D Bose gases, here we show that MI in 2D can support the critical formation of Townes solitons. Starting with a 2D superfluid of an initial density n_i and quenched to an attractive interaction $g_f < 0$, we show that MI causes collective modes with wavenumber around $k_{\text{MI}} = \pi/\xi$ associated with the interaction length (or ‘healing’ length) $\xi = \pi/\sqrt{2n_i|g_f|}$ to grow predominantly [17, 31, 32], fragmenting the superfluid as illustrated in Fig. 1(a). Intriguingly, the characteristic atom number in each wave packet $\sim n_i \xi^2 = \pi^2/2|g_f|$ well approaches the Townes threshold $N_{\text{th}} = 5.85/|g_f|$ [10], thus opening up a pathway for Townes soliton formation. This simple relation should apply universally for any n_i and g_f provided no other length scales set in. We note that, due to the scaling symmetry in 2D, a Townes soliton forms under a scale-invariant profile [6] and MI can set the physical length scale ξ .

In this letter, we report the observation of Townes solitons in quenched 2D Bose gases. We induce MI that breaks up an otherwise large 2D sample into fragments universally around the Townes threshold, forming solitary waves. We clearly identify solitary waves whose density distributions agree well with the Townes profiles – the stationary state solution of the 2D nonlinear Schrödinger equation (NLSE) [6, 10]. Our measurement further reveals universal solitary wave dynamics governed by the MI time scale and a universal scaling behavior in the density power spectra, allowing us to clearly identify a distinct time period for unstable growth of density waves (while conserving total atom number), followed by a short era of wave collapse and soliton formation. By performing second interaction quenches, we further examine collapse and expansion time scales of this intricate quasi-stationary state.

* Email: clhung@purdue.edu

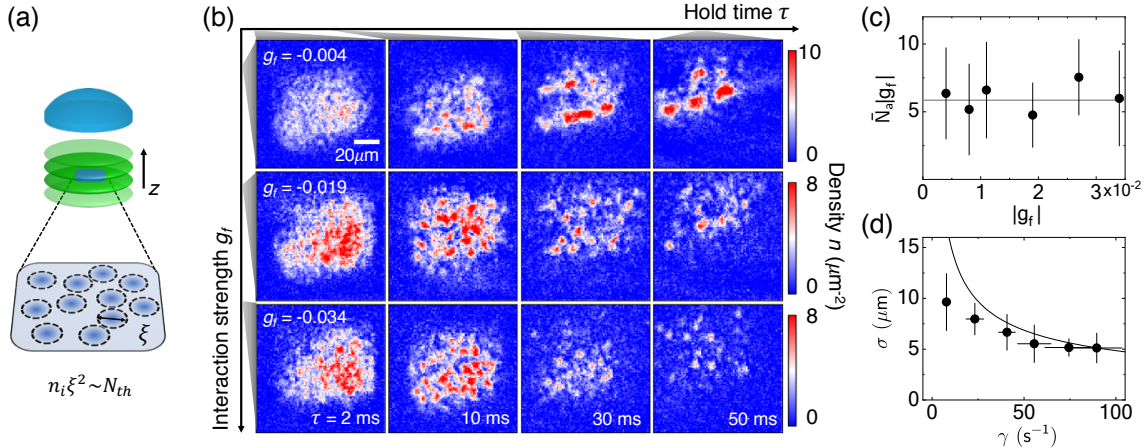


FIG. 1: Modulational instability and solitary wave formation in quenched 2D Bose gases. (a) Interaction quench-induced MI fragments a 2D gas (blue shaded square) into wave packets of a characteristic size ξ (dashed circles) that contains atom number $\sim n_i \xi^2$ approaching the Townes threshold N_{th} . The 2D gas is confined in a single node of a repulsive standing-wave potential (green shaded ovals), evolves for a hold time τ , and is imaged via a microscope objective (blue hemisphere); see Appendix A. (b) Single-shot images of samples quenched to the indicated interaction g_f (in each row) and held for the labeled time τ (in each column). Solitary waves (isolated density blobs) become visible at $\tau \geq 30$ ms. (c) Scaled mean atom number in a solitary wave $\bar{N}_a |g_f|$. Solid line marks the universal threshold $N_{th} |g_f| = 5.85$. (d) Mean size σ versus interaction energy $\hbar\gamma$. Solid line is the interaction length ξ . All data points in (c-d) are evaluated at $\tau = 42 \sim 50$ ms except for those of $g_f = -0.004$ which are evaluated at $\tau = 150 \sim 200$ ms. Error bars are standard errors.

II. INTERACTION QUENCH INDUCED SOLITARY WAVES AT THE TOWNES THRESHOLD

We begin the experiment with a uniform 2D superfluid formed by as many as $N \approx 1.5 \times 10^4$ cesium atoms trapped inside a quasi-2D box. The atomic surface density is $n_i \approx 5/\mu\text{m}^2$ and the surface area is controlled by a wall-like potential that is removed following the interaction quench (Appendix A). The tight vertical (z -) confinement of the box freezes all atoms in the harmonic ground state along z -axis. The trap vibrational level spacing ($\omega_z = 2\pi \times 1750$ Hz) is more than two orders of magnitude larger than the attractive interaction energy studied, ensuring that the observed wave dynamics is effectively 2D [33]. The initial interaction strength is tuned to $g_i = \sqrt{8\pi a/l_z} = 0.115$ via a magnetic Feshbach resonance [34], where a is the tunable s-wave scattering length and $l_z = 208$ nm is the vertical harmonic oscillator length.

We first induce MI in samples with a large surface area $A \approx (60 \mu\text{m})^2$. Following the interaction quench (in 1 ms) and a variable hold time τ , we perform single-shot absorption imaging to record the sample density distribution as shown in Fig. 1(b). Around 30 samples are imaged for ensemble analyses. In a short hold time, we observe density blobs randomly clumping up throughout a sample. The sizes of the blobs are smaller with larger $|g_f|$. At longer hold time, $\tau \geq 30$ ms, the number of observed blobs reduces, becoming more isolated, although the mean size and atom number of surviving blobs remain nearly unchanged for $\tau \leq 200$ ms; see also Appendix A.

We characterize these isolated blobs (solitary waves) and compare their atom number with the Townes threshold. We approximate their density profiles by 2D Gaussians [10] and fit the mean size σ and atom number \bar{N}_a . Within the interaction range studied, $-0.004 \geq g_f \geq -0.034$, in Fig. 1(c) we find that all rescaled atom numbers $\bar{N}_a |g_f|$ fall around the predicted Townes threshold $N_{th} |g_f| = 5.85$, giving a mean $\bar{N}_a |g_f| = 6(1)$. Interestingly, the standard deviation of the atom number δN_a scales with g_f accordingly, giving a mean fluctuation $\delta \bar{N}_a |g_f| = 3.2(5) \sim 0.5 \bar{N}_a |g_f|$. We believe that the number variation around the threshold results from the energy-time uncertainty relation, as we later show that these blobs form in a time scale $\sim \gamma^{-1}$, where $\hbar\gamma = \hbar^2 n_i |g_f|/m$ is the interaction energy, m is the atomic mass, and \hbar is the reduced Planck constant. While the average size and atom number of these solitary waves appear to evolve slowly within our experiment time (Appendix A), many of the observed soliton-like features should eventually collapse or expand after a long hold time. We will later address the evolution time scale when the atom number is driven significantly away from the Townes threshold (Fig. 6). Moreover, we show that the size of these solitary waves also agrees well with the prediction $\sigma \approx \xi$ in Fig. 1(d), indicating that MI provides the critical length scale for the possible formation of Townes solitons.

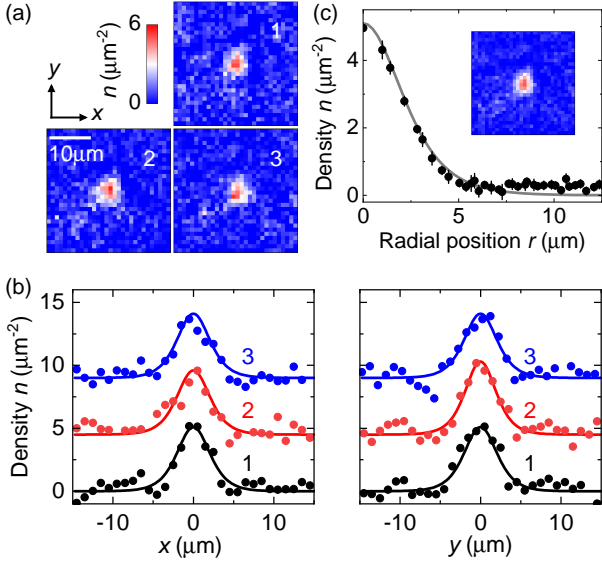


FIG. 2: Townes solitons and the Townes profiles. (a) Sample images of single solitary waves ($g_f = -0.034$) recorded at $\tau = 100$ ms. (b) Density line cuts (solid circles) through the center of images as numerically labeled in (a). Each data is offset by $4.5/\mu\text{m}^2$ for viewing. Solid lines are the Townes profiles of peak densities $n_0 = 5.1/\mu\text{m}^2$ (for #1,#3) and $5.8/\mu\text{m}^2$ (for #2), respectively. (c) Mean density image of (a) (inset: $30 \times 30 \mu\text{m}^2$) and the radial profile (solid circles) in close comparison with theory (solid curve) calculated using $n_0 = 5.1/\mu\text{m}^2$. Nearby dispersed blobs contribute to a small background at $r \gtrsim 7 \mu\text{m}$.

III. CONFIRMATION OF SOLITON FORMATION AND COMPARISON WITH THE TOWNES PROFILE

To confirm that some of the quench-induced solitary waves indeed form Townes solitons, we compare their density distributions with the scale-invariant, isotropic Townes profile [6]

$$n(r) = \frac{\alpha^2}{2|g_f|} |\phi(\alpha r)|^2, \quad (1)$$

where $\alpha = \sqrt{\frac{2n_0|g_f|}{|\phi(0)|^2}}$ is a scale factor. Given the peak density n_0 , the characteristic size and density profile of a Townes soliton are uniquely determined, or vice versa. Here, the radial function $\phi(\tilde{r})$ is the stationary solution of the scale-invariant 2D NLSE [6, 10]

$$\frac{d^2\phi}{d\tilde{r}^2} + \frac{1}{\tilde{r}} \frac{d\phi}{d\tilde{r}} + |\phi|^2 \phi - \phi = 0, \quad (2)$$

subject to the boundary conditions $\lim_{\tilde{r} \rightarrow \infty} \phi(\tilde{r}) = 0$ and $\frac{d\phi}{d\tilde{r}}|_{\tilde{r}=0} = 0$. The stationary profile $\phi(\tilde{r})$ has been evaluated numerically [6], giving $|\phi(0)| \approx 2.207$, and the norm $\int |\phi(\tilde{r})|^2 d\tilde{r} \approx 11.7$ sets the Townes threshold.

Figure 2 plots three isolated solitary waves of similar peak density $n_0 \sim n_i$ [56] that are randomly chosen from

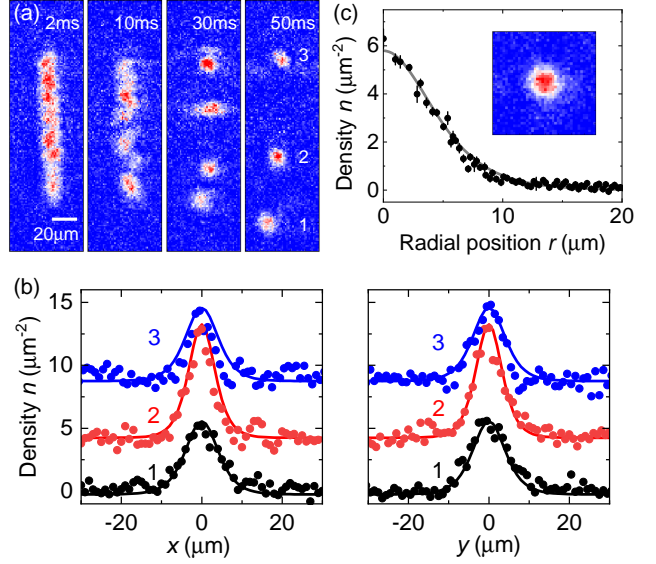


FIG. 3: Formation of a Townes soliton array. (a) Single-shot images of elongated samples quenched to $g_f = -0.0075$ and held for the labeled time τ . An array of fully isolated solitary waves become visible at $\tau \geq 30$ ms. (b) Density line cuts (solid circles) through the center of three solitary waves as numerically labeled in (a), each offset by $4.5/\mu\text{m}^2$ for viewing. Solid lines are the Townes profiles of $n_0 = 5.8/\mu\text{m}^2$ (for #1,#3) and $9/\mu\text{m}^2$ (for #2), respectively. (c) Mean density image of four randomly chosen solitons with $n_0 \approx 5.8/\mu\text{m}^2$ (inset: $40 \times 40 \mu\text{m}^2$) and the radial profile (solid circles), showing excellent agreement with theory (solid curve).

quenched samples ($g_f = -0.034$) at a long hold time $\tau = 100$ ms. Their individual density distributions, as well as the averaged radial density profile, indeed agree fairly well with the expected Townes profiles Eq. (1) with no fitting parameters. We note that, in the radial profile shown in Fig. 2(c), a small background is present at $r \gtrsim 7 \mu\text{m}$ due to dispersed blobs nearby. The observed close agreement with the Townes profiles should explain why these randomly chosen solitary waves, as well as those observed in Fig. 1, are long-lived.

To fully demonstrate that Townes solitons can generally form from our quench recipe, we induce MI in another set of 2D samples initially confined and then released from a narrow rectangular wall potential as shown in Fig. 3(a). We adjust the short side of the samples to be comparable to the MI length scale, so that a *single array* of solitons can form following the interaction quench. This avoids close proximity with many neighboring solitary waves or dispersing blobs, visible in large samples shown in Fig. 1(b). From these narrow samples, we clearly observe well-isolated solitary waves in almost every experiment repetition as shown in Fig. 3(a) at hold time $\tau \geq 30$ ms. In these solitary waves, we find ubiquitous agreement with the Townes profiles [Fig. 3(b-c)]. Together with Fig. 2, our observation confirms that Townes solitons can prevail from MI.

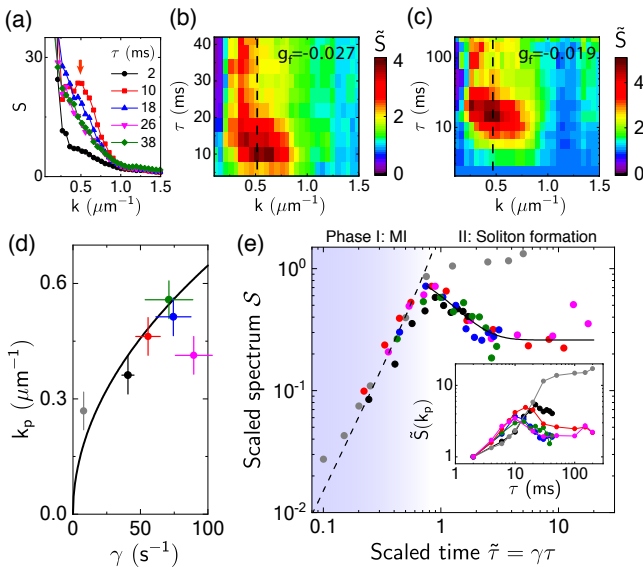


FIG. 4: Dynamics and universal scaling in the density power spectra. (a) Sample spectra $S(k, \tau)$ at $g_f = -0.027$ and the indicated hold time τ . (b) Corresponding growth spectra $\tilde{S}(k, \tau) = S(k, \tau)/S(k, \tau_0)$ with $\tau_0 = 2$ ms. (c) Sample growth spectra \tilde{S} at $g_f = -0.019$ and hold time up to 200 ms. Vertical dashed lines in (b-c) mark the peak wavenumber k_p . (d) k_p versus interaction energy $\hbar\gamma$ (filled circles) measured at $g_f = -0.004$ (gray), -0.011 (black), -0.019 (red), -0.027 (blue), and -0.034 (magenta and olive), respectively. Corresponding $\tilde{S}(k_p, \tau)$ are shown in the inset of (e). Solid line is the prediction $k_{\text{MI}} = \sqrt{2\gamma m/\hbar}$. Error bars include systematic and statistical errors. (e) Scaled spectra S plotted using Eq. (3), which collapse approximately onto a single curve except for the one at $g_f = -0.004$. Dashed line (Solid line) is a hyperbolic (exponential) fit to Phase I, $\tilde{\tau} < 0.8$ (II, $\tilde{\tau} > 0.8$), of the collapsed spectra; see text.

IV. MODULATIONAL INSTABILITY AND THE EVOLUTION OF DENSITY WAVES IN THE SOLITON FORMATION PROCESS

We now turn to study the dynamics of the soliton formation process, using the large-area samples discussed in Sec. II and Fig. 1. We evaluate the density power spectrum [36] $S(k, \tau) = \langle |n(k, \tau)|^2 \rangle / N$ in spatial frequency domain (momentum space) as a function of the hold time τ , using Fourier transform of the sample density distribution. Here $k = |\mathbf{k}|$ is the momentum wavenumber of the azimuthally averaged spectrum, N is the total atom number, and $\langle \cdot \rangle$ denotes ensemble averaging. In the power spectra (Fig. 4(a)), we clearly observe rapid growth of a nonzero momentum peak at short hold time (marked by an arrow), indicating the development of density waves at a dominant length scale throughout the sample. The nonzero momentum peak then dissipates at longer hold time until the power spectrum finally becomes monotonic and stationary, which signifies the collapse of density waves and fragmentation of the sample into solitons.

The evidence of MI-induced wave amplification at different interaction strengths is best illustrated when we plot the relative growth spectra $\tilde{S}(k, \tau) = S(k, \tau)/S(k, \tau_0)$, normalized by the initial power spectrum at $\tau_0 = 2$ ms. This allows us to determine which mode has the largest growth rate. For different samples in Figs. 4(b) and (c), the momentum peak is clearly visible within $0.2/\mu\text{m} < k < 1/\mu\text{m}$ at short hold time. The growth patterns look similar for samples with different g_f , although the peak location, height, and the evolution time scale vary. We identify the peak wavenumber k_p and find consistency with the prediction from MI in Fig. 4(d).

Another remarkable prediction from MI is that the power spectrum at k_p exhibits a universal time and amplitude scaling behavior with respect to the interaction time scale γ^{-1} . This is based on extending the Bogoliubov phonon picture to the regime under attractive interactions, which predicts that collective modes of opposite momenta are generated in pairs, as seeded from initial density perturbations, and subsequently form density waves along the associative directions while being amplified at a rate γ till significant depletion of the ground state atoms (Appendix B).

In Fig. 4(e), we experimentally test the scaling relation in the peak growth spectra $\tilde{S}(k_p, \tau)$, covering the entire evolution time period. We summarize the scaling relation as the following

$$\mathcal{S}(\tilde{\tau}) \approx \frac{\gamma}{\bar{\gamma}_i} [\tilde{S}(k_p, \tilde{\tau}) - 1], \quad (3)$$

where $\tilde{\tau} = \gamma\tau$ is the scaled time and $\mathcal{S}(\tilde{\tau})$ is the scaled spectrum. In the amplitude scaling, we normalize γ with the mean initial interaction energy unit $\bar{\gamma}_i = 306 \text{ s}^{-1}$ before the quench (Appendix B3). We show that six power spectra, each with different γ , can collapse onto a single curve over a surprisingly long scaled time $\tilde{\tau} < 10$. The only exception is the spectrum at $g_f = -0.004$, where we have used $\gamma^* = 3.2\gamma$ to force its collapse within $\tilde{\tau} \leq 0.8$. This different behavior is likely due to residual corrugations in the vertical confining trap influencing the dynamics, as the nonlinearity is weakest in this sample ($\gamma/2\pi \approx 1.2 \text{ Hz}$).

From this universal spectrum, we identify two distinct regimes of dynamics, divided by a critical time $\tilde{\tau}_c \approx 0.8$ as shown in Fig. 4(e). We label the time period $\tilde{\tau} \leq \tilde{\tau}_c$ for MI with an amplified (hyperbolic) growth of density waves (Appendix B2),

$$\tilde{S}(k_p, \tau) \approx 1 + \alpha \frac{\bar{\gamma}_i}{\gamma} \sinh^2(\gamma\tau), \quad (4)$$

where $\alpha = 1.5(1)$ is determined from a fit to $\mathcal{S}(\tilde{\tau})$ for $\tilde{\tau} \leq 0.5$; $\alpha = 2$ is obtained from the theory calculation for $\tilde{\tau} \ll 1$, neglecting the depletion of ground state atoms, dissipation, or interaction between the collective modes. Beyond $\tilde{\tau} \geq \tilde{\tau}_c$ after $\mathcal{S}(\tilde{\tau})$ reaches order of unity, dynamics enters the second phase, decaying with a time

constant $\Delta\tilde{\tau} \sim 0.8$ and transitioning to a slowly-evolving, quasi-stationary behavior.

Our data suggest the existence of a universal time and amplitude scaling behavior and a limit for the amplified density wave, followed by a universal dynamics for the wave collapse and soliton formation. For $g_f = -0.004$, however, $\tilde{S}(k_p, \tau)$ remains slowly-growing within $1 \leq \gamma^* \tau \leq 10$, suggesting less severe wave collapse.

V. SOLITON COLLISION DYNAMICS

Following the observed density wave collapse dynamics, a 2D sample fragments into many solitary wave packets of characteristic size $\sigma \sim \xi$. As seen in Fig. 1, due to close proximity of many wave packets (also with characteristic distances $\sim \xi$), collisions between them may induce collapses that lead to rapid atom number loss. Here, we show that MI time scale continues to dominate the collision dynamics and the total atom number loss in a quenched 2D Bose gas.

In a recent study of 1D soliton collisions [37], it is shown that merger occurs when solitons of similar phases collide, and two solitons of opposite phases appear to repel each other. In 2D, the merger of two soliton-like wave packets should lead to a new atom number $N_a > N_{\text{th}}$. This can induce collapse that quickly removes the merged soliton. For solitons or density blobs formed by MI with randomly seeded density waves in a large 2D sample, one expects no fixed phase relationship between neighbors. Merger can thus occur randomly throughout the sample and the total atom number loss may reveal the scaling of soliton binary collision losses.

In Fig. 5, we examine the total atom number loss for large samples quenched to different g_f (Fig. 1). We observe onset of loss in each sample at a time τ corresponding roughly to the critical time $\tilde{\tau}_c$, a behavior similarly observed for MI in 1D [18]. Beyond the critical time, we confirm that the loss curves can be well-captured by a simple two-body loss model, $\dot{N}/N = -\Gamma_{\text{2body}}N/A$. We attribute this behavior to the dominance of binary collisions between solitons or density blobs that trigger collapse and atom number loss; without triggered collapse, the usual three-body recombination loss should be negligible [38]. In Fig. 5(b), we find a linear dependence on $|g_f|$ in the measured loss coefficients Γ_{2body} . This in fact suggests a constant binary loss coefficient Γ_s for colliding wave packets, where $\Gamma_s = \Gamma_{\text{2body}}\bar{N}_a$ (Appendix C) and $\bar{N}_a|g_f| \approx 6$ is the measured universal number for solitary waves formed by MI.

We suspect this universal loss behavior results from MI scaling and 2D scale invariance, which suggests a constant binary loss coefficient,

$$\Gamma_s = \eta \frac{\hbar\pi}{m}, \quad (5)$$

independent of the interaction parameters (n_i, g_f) . This

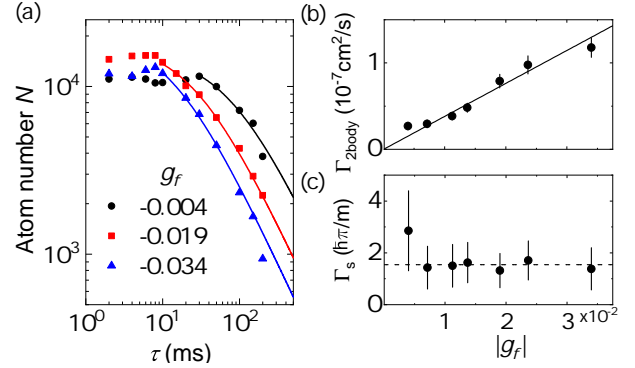


FIG. 5: Universal soliton collision dynamics in 2D. (a) Sample loss curves in total atom number N measured at the indicated interaction g_f . Solid lines are two-body loss fits after atom loss initiates. (b) Fitted rate coefficients. Solid line is a linear fit, giving a slope $\Gamma_{\text{2body}}/|g_f| = 3.8(2) \times 10^{-6} \text{ cm}^2/\text{s}$. (c) 2D soliton binary loss coefficients Γ_s determined from the rate coefficients in (b) and \bar{N}_a as in Fig. 1(c), and compared with the universal prediction Eq. (5), giving a mean $\eta = 1.5(1)$ (dashed line) and agreeing with $\eta = 1.5(3)$ alternatively determined from the fitted slope in (b) and mean $\bar{N}_a|g_f| = 6(1)$. Error bars are standard errors.

is because the collision rate $\Gamma_s \sim \sigma\bar{v}$ and the dependences on length scales in the linear cross-section $\sigma \approx \xi$ and relative velocity $\bar{v} \approx \sqrt{2}\hbar\pi/m\xi$ cancel each other; the constant $\eta \approx \sqrt{2}$ is estimated for $\sim 50\%$ probability of merger per collision or, equivalently, on average one soliton or density-blob loss per collision event. If Eq. (5) holds, we expect a collision lifetime $1/n_s\Gamma_s \sim \gamma^{-1}$, where $n_s = n_i/\bar{N}_a$ is the initial soliton/blob density (Appendix C). This suggests wave collapse and binary collision likely take place at the same rate during the second phase of the density evolution.

To unambiguously confirm the universality of collision dynamics, in Fig. 5(c) we deduce Γ_s independently using experimentally determined values $(\Gamma_{\text{2body}}, \bar{N}_a)$ at each g_f . Our results conform very well with the prediction by Eq. (5), giving a mean $\eta \approx 1.5$. We emphasize here that the loss coefficients universally depend only on the physical constants \hbar/m is a remarkable manifestation of MI and scale-invariant symmetry in 2D. The observations in Figs. 4 and 5 together confirm that interaction quench dynamics leads to Townes soliton formation at $\tau \gtrsim \gamma^{-1}$, followed by collision (that induces collapse) also at the same time scale γ^{-1} universally governed by MI.

VI. COLLAPSE AND EXPANSION DYNAMICS OF AN UNSTABLE TOWNES SOLITON

To gain further insight into the evolution of unstable Townes solitons, we determine their collapse and expansion time scales by driving the atom number more than three times away from the Townes threshold. To do this, we apply second interaction quench after solitons form at

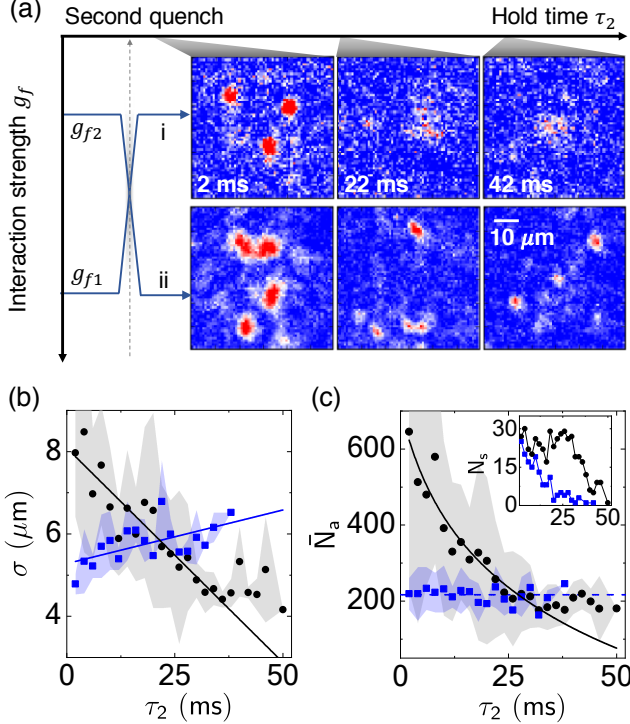


FIG. 6: Collapse and expansion dynamics following second interaction quenches. (a) Path i (ii): expansion (collapse) dynamics is initiated in solitons that are initially formed at $g_{f1} = -0.027$ (or $g_{f2} = -0.008$) followed by a second quench to g_{f2} (or g_{f1}). Single-shot sample images are recorded at the indicated hold time τ_2 after the second quench. (b-c) mean size σ and atom number \bar{N}_a versus τ_2 for paths i (blue squares) and ii (black circles), respectively. In (b), solid lines are linear fits, giving a collapse (expansion) rate $\dot{\sigma}/\gamma' \approx -1.8 \mu\text{m}$ (0.5 μm) normalized by the interaction energy unit $\gamma' = \hbar\bar{n}|g_{f2} - g_{f1}|/m \approx 55 \text{ s}^{-1}$ and $\bar{n} \approx 6/\mu\text{m}^2$ is mean initial peak density. In (c), blue dashed line marks the Townes threshold $N_{\text{th}} = 5.85/|g_{f1}|$. Black solid line is a guide to the eye, given by a tentative three-body loss fit (see text and Appendix D). Inset shows the observed soliton number N_s from the ensemble measurements. Shaded bands represent standard errors.

a sufficiently long hold time $\tau = 50 \text{ ms}$, hold for an additional time τ_2 , and perform imaging. In a quench path labeled (i) in Fig. 6(a) to a less attractive interaction, we induce immediate soliton expansion, during which \bar{N}_a remains constant, as expected, but the number of solitons N_s observed from the ensemble measurements greatly reduces; see Fig. 6(c) and inset. For a reversed quench path (ii) to a more attractive interaction, solitons collapse. In a short time scale $\gamma'^{-1} \sim 20 \text{ ms}$ corresponding to the interaction energy difference between the two quenches, we observe rapid reductions in both σ and \bar{N}_a .

In the collapse dynamics, we tentatively attribute the atom number loss within a soliton to few-body inelastic collisions that are primarily due to three-body recombination. However, in Fig. 6(c), we obtain an unphysical

loss coefficient that is five orders of magnitude larger than that measured in thermal samples [38]. A rapid three-body loss rate was also reported in the collapse within 1D solitons in a related experiment setting [18]. We believe that a more likely explanation for the rapid loss may be due to a combination of three-body loss under higher local collapse density and collective matter-wave ejection out of the solitons during the collapse [2, 39–41], which is challenging to detect given limited image resolution and signal-to-noise. Interestingly, the collapse seemingly slows down as \bar{N}_a drops to the new threshold value. We suspect either the atom loss has regulated the collapse, perhaps due to collective wave emission, or solitons with initial \bar{N}_a close to the new threshold survive. From the inset of Fig. 6(c), the observed continuing decrease of soliton number beyond $\tau_2 \geq 36 \text{ ms}$ may hint more of the latter case.

In either quench paths (i) and (ii), soliton evolution is clearly visible within the interaction time scale γ'^{-1} . For the dynamics after just a single quench, such rapid evolutions in mean atom number and soliton size are not observed. We therefore conclude that those surviving solitons formed by MI in a single quench are quasi-stationary within our experiment time $< 200 \text{ ms}$ as their norm are sufficiently close to the Townes threshold.

VII. CONCLUSION AND OUTLOOK

In summary, we study in detail the non-equilibrium dynamics and instability in 2D Bose gases quenched from repulsive to attractive interactions, and observe the dynamical formation of a quasi-stationary state – the Townes solitons. We observe MI in a 2D Bose gas that manifests as amplified pair-production of collective modes, as seeded by initial density perturbations. A hyperbolic growth of density waves results, exhibiting a universal scaling behavior and an amplification limit followed by universal wave collapse and fragmentation into solitary wave packets. We confirm that their norms and density distributions well-approach that of the Townes profiles and identify these wave packets as quasi-stationary Townes solitons.

MI-induced Townes solitons are observed to be collisionally unstable and are subject to collapse. However, further stabilization and manipulation may be possible by dynamically modulating the interaction [9, 42], confining in a harmonic trap [10] or adding a lattice potential [43, 44] as has been demonstrated to create 2D discrete solitons in nonlinear optics [11]. Future explorations of the final state dependences on the initial condition prior to the interaction quench may lead to interesting avenues such as the formation of vortex solitons [10, 45]. Lastly, we note that in the case of large initial sample size, boundary effect [32] does not seem to play a significant role in seeding the observed MI dynamics. Initial shape and size of the sample may however be manipulated to invoke strong boundary effects in

quench-induced MI, which is supported by our observation of a transiently aligned array of Townes solitons in Fig. 3. Combining with scale-invariance-breaking stabilization schemes, controlled formation of 2D solitons via

pair-production processes in MI may find future applications in matter-wave interferometry [46–48], or even the generation and distribution of many-body entanglement [49–52].

[1] P. A. Robinson, Nonlinear wave collapse and strong turbulence, *Rev. Mod. Phys.* **69**, 507 (1997).

[2] E. A. Donley, N. R. Claussen, S. L. Cornish, J. L. Roberts, E. A. Cornell, and C. E. Wieman, Dynamics of collapsing and exploding bose-einstein condensates, *Nature* **412**, 295 (2001).

[3] K. Moll, A. L. Gaeta, and G. Fibich, Self-similar optical wave collapse: observation of the townes profile, *Physical review letters* **90**, 203902 (2003).

[4] N. J. Zabusky and M. D. Kruskal, Interaction of “solitons” in a collisionless plasma and the recurrence of initial states, *Physical review letters* **15**, 240 (1965).

[5] A. Shabat and V. Zakharov, Exact theory of two-dimensional self-focusing and one-dimensional self-modulation of waves in nonlinear media, *Soviet physics JETP* **34**, 62 (1972).

[6] R. Y. Chiao, E. Garmire, and C. H. Townes, Self-trapping of optical beams, *Physical review letters* **13**, 479 (1964).

[7] L. Chomaz, L. Corman, T. Bienaimé, R. Desbuquois, C. Weitenberg, S. Nascimbène, J. Beugnon, and J. Dalibard, Emergence of coherence via transverse condensation in a uniform quasi-two-dimensional bose gas, *Nature communications* **6**, 6162 (2015).

[8] C.-L. Hung, X. Zhang, N. Gemelke, and C. Chin, Observation of scale invariance and universality in two-dimensional bose gases, *Nature* **470**, 236 (2011).

[9] Y. V. Kartashov, B. A. Malomed, and L. Torner, Solitons in nonlinear lattices, *Reviews of Modern Physics* **83**, 247 (2011).

[10] B. A. Malomed, Multidimensional solitons: Well-established results and novel findings, *The European Physical Journal Special Topics* **225**, 2507 (2016).

[11] J. W. Fleischer, M. Segev, N. K. Efremidis, and D. N. Christodoulides, Observation of two-dimensional discrete solitons in optically induced nonlinear photonic lattices, *Nature* **422**, 147 (2003).

[12] S. L. Cornish, S. T. Thompson, and C. E. Wieman, Formation of bright matter-wave solitons during the collapse of attractive bose-einstein condensates, *Physical review letters* **96**, 170401 (2006).

[13] Y. V. Kartashov, G. E. Astrakharchik, B. A. Malomed, and L. Torner, Frontiers in multidimensional self-trapping of nonlinear fields and matter, *Nature Reviews Physics* **1** (2019).

[14] Z. Chen, M. Segev, and D. N. Christodoulides, Optical spatial solitons: historical overview and recent advances, *Reports on Progress in Physics* **75**, 086401 (2012).

[15] P. Kevrekidis and D. Frantzeskakis, Pattern forming dynamical instabilities of bose-einstein condensates, *Modern Physics Letters B* **18**, 173 (2004).

[16] V. E. Zakharov and L. Ostrovsky, Modulation instability: the beginning, *Physica D: Nonlinear Phenomena* **238**, 540 (2009).

[17] A. H. Guth, M. P. Hertzberg, and C. Prescod-Weinstein, Do dark matter axions form a condensate with long-range correlation?, *Physical Review D* **92**, 103513 (2015).

[18] J. H. Nguyen, D. Luo, and R. G. Hulet, Formation of matter-wave soliton trains by modulational instability, *Science* **356**, 422 (2017).

[19] P. Everitt, M. Sooriyabandara, M. Guasoni, P. Wigley, C. Wei, G. McDonald, K. Hardman, P. Manju, J. Close, C. Kuhn, *et al.*, Observation of a modulational instability in bose-einstein condensates, *Physical Review A* **96**, 041601 (2017).

[20] K. Tai, A. Hasegawa, and A. Tomita, Observation of modulational instability in optical fibers, *Physical review letters* **56**, 135 (1986).

[21] D. Solli, G. Herink, B. Jalali, and C. Ropers, Fluctuations and correlations in modulation instability, *Nature Photonics* **6**, 463 (2012).

[22] J. M. Dudley, F. Dias, M. Erkintalo, and G. Genty, Instabilities, breathers and rogue waves in optics, *Nature Photonics* **8**, 755 (2014).

[23] K. E. Strecker, G. B. Partridge, A. G. Truscott, and R. G. Hulet, Formation and propagation of matter-wave soliton trains, *Nature* **417**, 150 (2002).

[24] L. Khaykovich, F. Schreck, G. Ferrari, T. Bourdel, J. Cubizolles, L. D. Carr, Y. Castin, and C. Salomon, Formation of a matter-wave bright soliton, *Science* **296**, 1290 (2002).

[25] V. V. Konotop and M. Salerno, Modulational instability in bose-einstein condensates in optical lattices, *Phys. Rev. A* **65**, 021602 (2002).

[26] I. Carusotto, D. Embriaco, and G. C. La Rocca, Nonlinear atom optics and bright-gap-soliton generation in finite optical lattices, *Physical Review A* **65**, 053611 (2002).

[27] O. Morsch and M. Oberthaler, Dynamics of bose-einstein condensates in optical lattices, *Rev. Mod. Phys.* **78**, 179 (2006).

[28] A. Campillo, S. Shapiro, and B. Suydam, Relationship of self-focusing to spatial instability modes, *Applied Physics Letters* **24**, 178 (1974).

[29] A. V. Mamaev, M. Saffman, D. Z. Anderson, and A. A. Zozulya, Propagation of light beams in anisotropic nonlinear media: From symmetry breaking to spatial turbulence, *Phys. Rev. A* **54**, 870 (1996).

[30] Y. S. Kivshar and D. E. Pelinovsky, Self-focusing and transverse instabilities of solitary waves, *Physics Reports* **331**, 117 (2000).

[31] L. Salasnich, A. Parola, and L. Reatto, Modulational instability and complex dynamics of confined matter-wave solitons, *Physical review letters* **91**, 080405 (2003).

[32] L. D. Carr and J. Brand, Spontaneous soliton formation and modulational instability in bose-einstein condensates, *Physical review letters* **92**, 040401 (2004).

[33] P. Pedri and L. Santos, Two-dimensional bright solitons in dipolar bose-einstein condensates, *Physical review letters* **95**, 200404 (2005).

[34] C. Chin, R. Grimm, P. Julienne, and E. Tiesinga, Fes-

hbach resonances in ultracold gases, *Reviews of Modern Physics* **82**, 1225 (2010).

[35] Since MI sets the physical length scale during the soliton formation process, $\alpha \sim \xi^{-1}$, the peak density of most solitons should be comparable to the initial sample density $n_0 \sim n_i$.

[36] C.-L. Hung, V. Gurarie, and C. Chin, From cosmology to cold atoms: Observation of sakharov oscillations in a quenched atomic superfluid, *Science* **341**, 1213 (2013).

[37] J. H. Nguyen, P. Dyke, D. Luo, B. A. Malomed, and R. G. Hulet, Collisions of matter-wave solitons, *Nature Physics* **10**, 918 (2014).

[38] T. Kraemer, M. Mark, P. Waldburger, J. G. Danzl, C. Chin, B. Engeser, A. D. Lange, K. Pilch, A. Jaakkola, H.-C. Nägerl, *et al.*, Evidence for efimov quantum states in an ultracold gas of caesium atoms, *Nature* **440**, 315 (2006).

[39] Y. Kagan, A. E. Muryshev, and G. V. Shlyapnikov, Collapse and bose-einstein condensation in a trapped bose gas with negative scattering length, *Physical review letters* **81**, 933 (1998).

[40] H. Saito and M. Ueda, Intermittent implosion and pattern formation of trapped bose-einstein condensates with an attractive interaction, *Physical review letters* **86**, 1406 (2001).

[41] H. Saito and M. Ueda, Mean-field analysis of collapsing and exploding bose-einstein condensates, *Physical Review A* **65**, 033624 (2002).

[42] H. Saito and M. Ueda, Dynamically stabilized bright solitons in a two-dimensional bose-einstein condensate, *Physical review letters* **90**, 040403 (2003).

[43] N. K. Efremidis, J. Hudock, D. N. Christodoulides, J. W. Fleischer, O. Cohen, and M. Segev, Two-dimensional optical lattice solitons, *Physical review letters* **91**, 213906 (2003).

[44] B. B. Baizakov, B. A. Malomed, and M. Salerno, Multidimensional solitons in a low-dimensional periodic potential, *Physical Review A* **70**, 053613 (2004).

[45] L. Carr and C. W. Clark, Vortices in attractive bose-einstein condensates in two dimensions, *Physical review letters* **97**, 010403 (2006).

[46] A. D. Cronin, J. Schmiedmayer, and D. E. Pritchard, Optics and interferometry with atoms and molecules, *Reviews of Modern Physics* **81**, 1051 (2009).

[47] R. Bücker, J. Grond, S. Manz, T. Berrada, T. Betz, C. Koller, U. Hohenester, T. Schumm, A. Perrin, and J. Schmiedmayer, Twin-atom beams, *Nature Physics* **7**, 608 (2011).

[48] B. Lücke, M. Scherer, J. Kruse, L. Pezzé, F. Deuretzbacher, P. Hyllus, J. Peise, W. Ertmer, J. Arlt, L. Santos, *et al.*, Twin matter waves for interferometry beyond the classical limit, *Science* **334**, 773 (2011).

[49] C. Gross, H. Strobel, E. Nicklas, T. Zibold, N. Bar-Gill, G. Kurizki, and M. Oberthaler, Atomic homodyne detection of continuous-variable entangled twin-atom states, *Nature* **480**, 219 (2011).

[50] K. Lange, J. Peise, B. Lücke, I. Kruse, G. Vitagliano, I. Apellaniz, M. Kleinmann, G. Tóth, and C. Klempt, Entanglement between two spatially separated atomic modes, *Science* **360**, 416 (2018).

[51] P. Kunkel, M. Prüfer, H. Strobel, D. Linnemann, A. Frölian, T. Gasenzer, M. Gärttner, and M. K. Oberthaler, Spatially distributed multipartite entanglement enables epr steering of atomic clouds, *Science* **360**, 413 (2018).

[52] M. Fadel, T. Zibold, B. Décamps, and P. Treutlein, Spatial entanglement patterns and einstein-podolsky-rosen steering in bose-einstein condensates, *Science* **360**, 409 (2018).

[53] C.-L. Hung, X. Zhang, L.-C. Ha, S.-K. Tung, N. Gemelke, and C. Chin, Extracting density-density correlations from in situ images of atomic quantum gases, *New Journal of Physics* **13**, 075019 (2011).

[54] L. Feng, L. W. Clark, A. Gaj, and C. Chin, Coherent inflationary dynamics for bose-einstein condensates crossing a quantum critical point, *Nature Physics* **14**, 269 (2018).

[55] L. Pitaevskii and S. Stringari, *Bose-Einstein condensation and superfluidity*, Vol. 164 (Oxford University Press, 2016).

[56] Since MI sets the physical length scale during the soliton formation process, $\alpha \sim \xi^{-1}$, the peak density of most solitons should be comparable to the initial sample density $n_0 \sim n_i$.

Acknowledgments

We acknowledge discussions with Qi Zhou, Chih-Chun Chien, Sergei Khlebnikov, and Chris Greene. We thank Cheng Chin for discussions and many critical comments. We are grateful to H. J. Kimble for instrument loan since the early stage of this project. We thank May Kim, Yiyang Fang, and Wuxiucheng Wang for laboratory assistance. This project is supported in part by the Purdue Research Foundation, the W. M. Keck Foundation, the NSF Award PHY-1848316, and the U.S. Department of Energy (grant# DE-SC0019202).

Appendix A: Experimental procedures

1. Formation of uniform 2D Bose gases

Figure A1 shows the schematics of the experiment. Our uniform 2D Bose gas is confined in a quasi-2D box potential formed by all repulsive optical dipole beams. The vertical box confinement is provided by a single node of a repulsive standing-wave potential ($2 \mu\text{m}$ periodicity) along the vertical (z -) direction. The node defines the horizontal 2D plane. The measured vertical trap frequency in the node is $\omega_z/2\pi = 1.75(2) \text{ kHz} \gg (k_B T, |\mu|)/\hbar$, freezing all atoms in the harmonic ground state. Here k_B is the Boltzmann constant, $T \leq 8 \text{ nK}$ is the temperature measured in time-of-flight, and μ is the chemical potential. The horizontal boundary of the box is formed by a tightly focused repulsive optical beam that scans the box boundary to form a time-averaged wall potential. The beam is controlled by a pair of acousto-optic deflector and is projected through the same microscope objective (numerical aperture N.A. = 0.37) used for imaging (resolution $< 2 \mu\text{m}$).

We perform the interaction quench while simultaneously removing the wall potential to allow hot collision products (due to soliton collapses) to eject out of the experiment field of view. When the wall potential is removed, the residual global trap frequency in the horizontal plane, due to a weak magnetic trap, is experimentally determined to be $\omega_r/2\pi < 1.5 \text{ Hz}$ through superfluid dipole oscillations.

2. Magnetic two-body interaction tuning

The scattering length is tuned using a magnetic Feshbach resonance [34, 38]. We identify zero scattering length at the magnetic field $B = 17.120(6)\text{G}$, using the superfluid in-situ size as well as the expansion rate in a 2D time-of-flight. We adopt the formula [38] $a(B) = (1722 + 1.52B/G) \left(1 - \frac{\Delta B}{B/G - B_0}\right)$ for the scattering length conversion, where $\Delta B = 28.72$ and $B_0 = -11.60$ is adjusted to shift the zero-crossing to the measured value.

3. Solitary wave characterization in a large sample

To identify and characterize a solitary wave at long hold time in samples as shown in Fig. 1, we search for isolated blobs with peak density above a threshold around 80% of the initial density n_i , and then fit each blob with a 2D Gaussian in approximation to the Townes profile [6]. From each fit, we obtain the root-mean-square (r.m.s.) diameters and extract the atom number \bar{N}_a under the fitted density profile. We then evaluate the mean size σ and atom number \bar{N}_a . Examples at long hold time $\tau \geq 50 \text{ ms}$ can be found in Fig. A2, which shows no signs

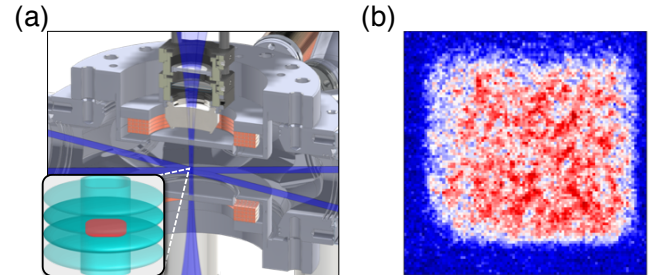


Fig. A1: (a) Schematic of the experiment showing two crossed vertical confinement beams (blue shaded sheets) and the wall beam (blue shaded cylinder). Inset illustrates a 2D gas (red shaded square) confined in the box potential, which is represented by a single node between the blue shaded ovals with the square-wall cylinder beam forming the box boundary. (b) Single-shot sample image of a 2D gas loaded in the box potential. Image size is $90 \times 90 \mu\text{m}^2$ and pixel size is $1 \mu\text{m}^2$.

of rapid collapse or expansion in the mean size and atom number following a single interaction quench.

Appendix B: Quench-induced dynamics in the density power spectrum

In a 2D gas with uniform mean density distribution, the density power spectrum at finite k is essentially the density static structure factor, which is the Fourier transform of the density-density correlation function [53]. In the following, we discuss the quench evolution of the static structure factor (density power spectrum) measured in our samples, while neglecting density perturbations due to boundary effects.

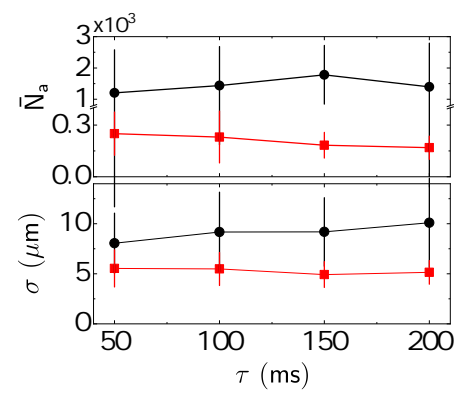


Fig. A2: Mean atom number \bar{N}_a and root-mean-square diameter σ versus hold time τ measured at $g_f = -0.004$ (black circles) and -0.019 (red squares), respectively. Error bars are standard errors.

1. Theory of density structure factor after an interaction quench to $g_f < 0$

For a Bose superfluid with initial density n_i immediately following the interaction quench, we expect density waves with wavenumber $0 < k < \sqrt{4|g_f|n_i}$ to grow unstably since the usual Bogoliubov dispersion becomes purely imaginary. There is no straightforward theory for evaluating quench evolution at all hold time τ . To gain insights, here we analytically evaluate the quench dynamics only in the very early stage when most of the atoms still remain in the zero momentum state. We focus on the time-evolution of the static structure factor [36, 54]. Analytically, it can be evaluated as

$$S(\mathbf{k}) = \frac{1}{N} \sum_{\mathbf{q}, \mathbf{q}'} \langle \hat{a}_{\mathbf{q}+\mathbf{k}}^\dagger \hat{a}_{\mathbf{q}} \hat{a}_{\mathbf{q}'-\mathbf{k}}^\dagger \hat{a}_{\mathbf{q}'} \rangle, \quad (\text{B1})$$

where $\hat{a}_{\mathbf{k}}(\hat{a}_{\mathbf{k}}^\dagger)$ stands for the annihilation (creation) operator of a momentum state $|\mathbf{k}\rangle$ and N is the total atom number. At very short hold time $\tau \ll \gamma^{-1}$, the Bose gas is still primarily populated by ground state atoms ($\hat{a}_0^{(\dagger)} \approx \sqrt{N}$), where $\hbar\gamma = \hbar^2 n_i |g_f|/m$ is the interaction energy, m is the atomic mass, and \hbar is the reduced Planck constant. The structure factor reduces to

$$S(\mathbf{k}) = \langle \hat{a}_{\mathbf{k}}^\dagger \hat{a}_{\mathbf{k}} \rangle + \langle \hat{a}_{-\mathbf{k}} \hat{a}_{-\mathbf{k}}^\dagger \rangle + \langle \hat{a}_{\mathbf{k}}^\dagger \hat{a}_{-\mathbf{k}}^\dagger \rangle + \langle \hat{a}_{-\mathbf{k}} \hat{a}_{\mathbf{k}} \rangle. \quad (\text{B2})$$

We perform the following transformation for momentum state within the range $0 < |\mathbf{k}| < \sqrt{4|g_f|n_i}$, expressing the momentum state operator with a set of bosonic mode operators $\hat{b}_{\mathbf{k}}$ ($\hat{b}_{-\mathbf{k}}^\dagger$) as

$$\begin{aligned} \hat{a}_{\mathbf{k}} &= i \left[u_k \hat{b}_{\mathbf{k}} + v_k \hat{b}_{-\mathbf{k}}^\dagger \right] \\ \hat{a}_{-\mathbf{k}}^\dagger &= -i \left[v_k \hat{b}_{\mathbf{k}} + u_k \hat{b}_{-\mathbf{k}}^\dagger \right]. \end{aligned} \quad (\text{B3})$$

Here, we set the coefficients $u_k = \sqrt{\frac{\hbar\gamma}{2\epsilon(k)} + \frac{1}{2}}$ and $v_k = \sqrt{\frac{\hbar\gamma}{2\epsilon(k)} - \frac{1}{2}}$, $\epsilon(k) = \sqrt{|\epsilon_k^2 - 2\epsilon_k \hbar\gamma|}$ is the imaginary part of the Bogoliubov energy, and $\epsilon_k = \hbar^2 k^2 / 2m$ is the single particle dispersion. $\hat{b}_{\mathbf{k}}$ ($\hat{b}_{-\mathbf{k}}^\dagger$) obeys the usual bosonic commutation relation. Using procedures similar to the standard Bogoliubov transformation, we can recast the weakly-interacting Hamiltonian into the following form

$$\hat{H} = \frac{N\mu}{2} + \sum_{\mathbf{k} \neq 0} \epsilon(k) (\hat{b}_{\mathbf{k}}^\dagger \hat{b}_{-\mathbf{k}}^\dagger + \hat{b}_{\mathbf{k}} \hat{b}_{-\mathbf{k}}) - \sum_{\mathbf{k} \neq 0} \left(\frac{\hbar^2 k^2}{2m} + \mu \right), \quad (\text{B4})$$

where the summation runs over half of momentum space and $\mu = -\hbar\gamma$ is the chemical potential. Note that, under this transformation, new excitations are generated (and also annihilated) in pairs as hold time increases. In the Heisenberg picture, these operators obey a set of coupled equations of motion, $\dot{\hat{b}}_{\mathbf{k}} = \frac{i}{\hbar} [\hat{H}, \hat{b}_{\mathbf{k}}] = -\frac{i}{\hbar} \epsilon(k) \hat{b}_{-\mathbf{k}}^\dagger$ and its Hermitian conjugate, which lead to the following solution

$$\hat{b}_{\mathbf{k}} = \hat{b}_{0,\mathbf{k}} \cosh \frac{\epsilon(k)\tau}{\hbar} - i \hat{b}_{0,-\mathbf{k}}^\dagger \sinh \frac{\epsilon(k)\tau}{\hbar} \quad (\text{B5})$$

$$\hat{b}_{-\mathbf{k}}^\dagger = \hat{b}_{0,-\mathbf{k}}^\dagger \cosh \frac{\epsilon(k)\tau}{\hbar} + i \hat{b}_{0,\mathbf{k}} \sinh \frac{\epsilon(k)\tau}{\hbar}, \quad (\text{B6})$$

and $\hat{b}_{0,\mathbf{k}}(\hat{b}_{0,-\mathbf{k}}^\dagger)$ is the bosonic mode operator at time $\tau = 0$ right after the interaction quench. Plugging this solution into Eq. (B3) and evaluate the structure factor Eq. (B2), we then find the following time-dependent evolution

$$\begin{aligned} S(\mathbf{k}, \tau) &= \frac{\epsilon_k}{\epsilon(k)} \left[\langle \hat{b}_{0,\mathbf{k}}^\dagger \hat{b}_{0,\mathbf{k}} \rangle + \langle \hat{b}_{0,-\mathbf{k}} \hat{b}_{0,-\mathbf{k}}^\dagger \rangle \cosh 2 \frac{\epsilon(k)\tau}{\hbar} \right. \\ &\quad \left. - \langle \hat{b}_{0,\mathbf{k}}^\dagger \hat{b}_{0,-\mathbf{k}}^\dagger \rangle + \langle \hat{b}_{0,-\mathbf{k}} \hat{b}_{0,\mathbf{k}} \rangle \right) \\ &\quad - i \left(\langle \hat{b}_{0,\mathbf{k}}^\dagger \hat{b}_{0,-\mathbf{k}}^\dagger \rangle - \langle \hat{b}_{0,-\mathbf{k}} \hat{b}_{0,\mathbf{k}} \rangle \right) \sinh 2 \frac{\epsilon(k)\tau}{\hbar} \right]. \quad (\text{B7}) \end{aligned}$$

Here, the first line contains mode contributions that are seeded by the initial bosonic mode populations right after the quench. These modes grow ‘hyperbolically’ in the early stage of the quench dynamics. The second and third lines contain the contributions from mode populations that are generated or annihilated from the interaction quench, where the hyperbolic term is expected to vanish, leaving only the constant term (see below).

2. Amplification of density waves from density fluctuations prior to the quench

By using Eq. (B3) and the Bogoliubov transformation, we can further relate the expectation values of the bosonic modes in Eq. (B7) to those of the phonon modes before the interaction quench. We find

$$\langle \hat{b}_{0,\mathbf{k}}^\dagger \hat{b}_{0,\mathbf{k}} \rangle + \langle \hat{b}_{0,-\mathbf{k}} \hat{b}_{0,-\mathbf{k}}^\dagger \rangle = \epsilon_k \frac{\hbar(\gamma_i + \gamma)}{\epsilon_i(k)\epsilon(k)} \zeta \quad (\text{B8})$$

$$\langle \hat{b}_{0,\mathbf{k}}^\dagger \hat{b}_{0,-\mathbf{k}}^\dagger \rangle = \langle \hat{b}_{0,\mathbf{k}} \hat{b}_{0,-\mathbf{k}} \rangle = \frac{\epsilon_k^2 + \epsilon_k \hbar(\gamma_i - \gamma)}{2\epsilon_i(k)\epsilon(k)} \zeta, \quad (\text{B9})$$

and

$$\zeta = \langle \hat{c}_{0,\mathbf{k}}^\dagger \hat{c}_{0,\mathbf{k}} \rangle + \langle \hat{c}_{0,-\mathbf{k}} \hat{c}_{0,-\mathbf{k}}^\dagger \rangle. \quad (\text{B10})$$

Here, $\hat{c}_{0,\mathbf{k}}(\hat{c}_{0,\mathbf{k}}^\dagger)$ is the phonon annihilation (creation) operator, $\epsilon_i(k) = \sqrt{\epsilon_k^2 + 2\epsilon_k \hbar\gamma_i}$ is the Bogoliubov dispersion at interaction $g_i > 0$ prior to the quench, $\gamma_i = \hbar n_i g_i / m$, and we have used $\langle \hat{c}_{0,\mathbf{k}}^\dagger \hat{c}_{0,-\mathbf{k}}^\dagger \rangle = \langle \hat{c}_{0,\mathbf{k}} \hat{c}_{0,-\mathbf{k}} \rangle = 0$ in the above relation since there is no source or sink for phonons in our 2D gas. It is clear that the bosonic mode population Eqs. (B8-B9) is seeded by the initial thermal phonon population and zero-point fluctuations

$$\langle \hat{c}_{0,\mathbf{k}}^\dagger \hat{c}_{0,\mathbf{k}} \rangle + \langle \hat{c}_{0,-\mathbf{k}} \hat{c}_{0,-\mathbf{k}}^\dagger \rangle = \frac{2}{e^{\epsilon_i(k)/k_B T} - 1} + 1 = \coth \frac{\epsilon_i(k)}{2k_B T}. \quad (\text{B11})$$

Using the above relations and keeping only the wavenumber k -dependence, Eq. (B7) can now be simplified as

$$S(k, \tau) = S_0(k) \left[1 + \frac{2\epsilon_k \hbar(\gamma_i + \gamma)}{\epsilon(k)^2} \sinh^2 \frac{\epsilon(k)\tau}{\hbar} \right], \quad (\text{B12})$$

where the overall factor

$$S_0(k) = \frac{\hbar^2 k^2}{2m\epsilon_i(k)} \coth \frac{\epsilon_i(k)}{2k_B T} \quad (\text{B13})$$

is exactly the equilibrium static structure factor [55] right before the interaction quench.

3. The scaling behavior

In Eq. (B12), the second term in the bracket represents contributions from the MI-amplified density waves, suggesting density waves at wavenumber $k_p = \sqrt{2|g_f|n_i}$ have the largest amplification rate $\epsilon(k_p)/\hbar = \gamma$. Thus, at short hold time $\tau \ll \gamma^{-1}$, we expect the growth of density power spectrum $\tilde{S}(k_p, \tau) \equiv S(k_p, \tau)/S(k_p, 0)$ to obey the following scaling relation

$$S(\tilde{\tau}) = \zeta \left[\tilde{S}(k_p, \tilde{\tau}) - 1 \right], \quad (\text{B14})$$

where $\tilde{\tau} = \gamma\tau$ is the scaled time, $\zeta = \frac{\gamma}{\gamma_i + \gamma}$ is a dimensionless amplitude scaling factor, and $\tilde{S}(\tilde{\tau})$ is the scaled spectrum; $\zeta \approx \gamma/\gamma_i$ when $\gamma_i \gg \gamma$. The scaled spectrum should display a universal hyperbolic growth at short hold time

$$S(\tilde{\tau}) = 2 \sinh^2(\tilde{\tau}). \quad (\text{B15})$$

4. Relationship with quench dynamics at $g_f > 0$

We note that the time-dependent density power spectrum Eq. (B12) is essentially the analytical continuation of quench-induced Sakharov oscillations in the static structure factor at $g_f > 0$ [36],

$$S(k, \tau) = S_0(k) \left[1 + \frac{\epsilon_i(k)^2 - \epsilon^2(k)}{\epsilon(k)^2} \sin^2 \frac{\epsilon(k)\tau}{\hbar} \right], \quad (\text{B16})$$

where now a coherent, sinusoidal oscillation in the structure factor replaces the hyperbolic growth. The calculation is in principle valid for all hold time τ for $g_f > 0$, in contrast to the case of $g_f < 0$, provided no global trap effect or other effects set in.

5. Experimental test of the scaling behavior in the density power spectrum

We experimentally test the scaling behavior Eq. (B14) over an extended time period. We have empirically searched for the best amplitude scaling relation ζ for a larger time range $0 < \tilde{\tau} < 5$. We find that the spectra scale the best with $\zeta \propto \gamma$, keeping explicit dependence on $n_i|g_f|$. We adopt a simple amplitude scaling factor $\zeta = \gamma/\bar{\gamma}_i$, using mean $\bar{\gamma}_i = \hbar\bar{n}_i g_i/m = 306 \text{ s}^{-1}$ evaluated from all samples (mean $\bar{n}_i = 6/\mu\text{m}^2$ and standard

deviation $\delta n_i = 1/\mu\text{m}^2$). We note that an alternative amplitude scaling factor $\zeta = \gamma/(\bar{\gamma}_i + \gamma)$ close to the exact form in Eq. (B14) gives a similar data collapse as in Fig. 4(e).

Appendix C: Soliton collision dynamics

1. Soliton binary collision coefficient Γ_s

Binary collisions between solitons can lead to merger [37], which makes soliton atom number $N_a > N_{\text{th}}$ much greater than the Townes threshold and induces collapse and rapid atom loss. Soliton binary loss behavior can be effectively described by $\dot{N}_s/N_s = -\Gamma_s n_s$, where N_s is the number of solitons, $n_s = N_s/A$ is the surface density, and Γ_s is the 2D binary loss coefficient as discussed in the main text. For total atom number loss dominated by soliton binary collision loss, we should have $\dot{N}/N = -\Gamma_{\text{2body}} n$, where n is the atom number density. We convert the soliton number into total atom number N using $N_s = N/\bar{N}_a$ [18, 19] and assuming \bar{N}_a is approximately constant over the experiment time. We find the simple relation $\Gamma_s = \Gamma_{\text{2body}} \bar{N}_a$, relating the measured loss coefficient Γ_{2body} to the binary collision coefficient Γ_s .

2. Collision lifetime of solitons

Following the determination of universal collision dynamics, we also obtain the collision lifetime of solitons right after the formation process near $\tilde{\tau} \approx \tilde{\tau}_c$. We calculate the lifetime $\Delta\tau_s = \frac{1}{\Gamma_s n_s} \approx \frac{m\bar{N}_a}{\eta\pi\hbar n_i} \approx \gamma^{-1}$, where we have used $n_s = n_i/\bar{N}_a$, the measured universal threshold $\bar{N}_a|g_f| = 6$ (Fig. 1), and the measured constant $\eta = 1.5$ (Fig. 5).

Appendix D: Fitting atom number loss during rapid soliton collapse

Following the second interaction quench in path (ii) as shown in Fig. 6, mean atom number in a soliton $\bar{N}_a(\tau_2 = 0)$ exceeds the new Townes threshold by three-fold and solitons begin to collapse. From the linear fit in Fig. 6(b), we obtain an approximate linear time-dependent size $\sigma(\tau_2) = \sigma_0 + \dot{\sigma}\tau_2$, where $\sigma_0 = 8.0 \mu\text{m}$ and $\dot{\sigma} = -0.11 \text{ mm/s}$. Here we consider a simple case where the atom number loss within a soliton is fully due to three-body recombination. Because the vertical oscillator length $l_z = 208 \text{ nm}$ far exceeds the magnitude of the 3D scattering length $|a| = 1.1 \text{ nm}$, we expect the three-body loss behavior to be 3D in nature. To quantify the three-body loss rate, we develop a model that takes into account the shrinking soliton size in the 2D plane, while assuming that the vertical wave packet remains in

the harmonic ground state. This is justified because the 2D density n needs to increase by ~ 170 times for the interaction energy to approach the vertical trap vibrational energy. Such dramatic increase in 2D density is not observed in our images, where the soliton size remains larger than the image resolution during the time of collapse. We therefore adopt the standard three-body recombination loss model

$$\frac{d\bar{N}_a}{d\tau_2} = -\frac{L_3}{9\sqrt{3}\pi^3\sigma(\tau_2)^4l_z^2}\bar{N}_a^3, \quad (\text{D1})$$

where L_3 is the three-body loss coefficient and we have used a Gaussian form to approximate the soliton 3D density profile. From the above equations and the approximate linear time-dependence in σ , we derive an analytical formula

$$\bar{N}_a(\tau_2) = \frac{\bar{N}_a(0)}{\sqrt{1 + \frac{2L_3\bar{N}_a(0)^2}{27\sqrt{3}\pi^3l_z^2|\dot{\sigma}|} \left[\frac{1}{(\sigma_0 + \dot{\sigma}\tau_2)^3} - \frac{1}{\sigma_0^3} \right]}}, \quad (\text{D2})$$

where L_3 is the fit parameter. This effective three-body loss model appears to fit our data except beyond $\tau_2 > 36$ ms when the atom number reaches the new Townes threshold. The fitted $L_3 = 1.1(1) \times 10^{-23}$ cm⁶/s is nonetheless five orders of magnitude larger than that measured in a thermal sample [38], which we believe is not physical. To reconcile this discrepancy may require a different collapse dynamics that, for example, creates three-body loss under higher local collapse density beyond our image resolution and also rapidly ejects atoms out of a collapsing soliton [2, 39–41].